



Effects of anisotropy and boundary plates on the critical values of a porous medium heated from below

Michael R. Gustafson II, Laurens E. Howle*

Department of Mechanical Engineering and Materials Science, Center for Nonlinear and Complex Systems, Duke University, Durham, NC 27708, USA

Received 13 January 1998; received in revised form 4 January 1999

Abstract

We present a linear stability analysis of Horton–Rogers–Lapwood convection in an anisotropic porous medium bounded by finite-property plates of infinite horizontal extent. Critical values for the onset of convection are obtained using a continuation method. These values are compared with experimental data. The effects of plate diffusivity, plate thickness, and anisotropy in the diffusivity and permeability of the porous medium on these critical values are explored. We find that the predicted critical values from our stability analysis agree favorably with available precision experimental measurements. © 1999 Elsevier Science Ltd. All rights reserved.

1. Introduction

The field of natural convection has received a great deal of experimental and analytical attention in recent years as scientists and engineers discover new systems in which it plays a role. Specific areas include convection in the ‘mushy zone’ during the solidification of alloys and fluid transport through soils. An overview of these areas can be found in the literature [1,2].

The particular topic of a fluid-saturated porous medium heated from below was first studied by Horton and Rogers [3] in 1945. Three years later, Lapwood [4] independently wrote about natural convection in a porous medium and whether or not convective currents could be sustained. Since then, much theory has been presented on natural convection in a fluid-saturated porous medium enclosed by ideal horizontal boundaries. The term ‘ideal’ in this case refers to a boundary that is infinitely conductive and has no thickness. Experimentally, however, the properties of the bound-

aries themselves may affect the critical values (critical wave number and Rayleigh number) of the fluid-saturated porous medium. Riahi [5] has studied how conducting boundaries can affect convection, but he assumed that the boundaries had no thickness. In this paper, however, we allow the boundaries to have a finite thickness as well as a finite conductivity. The particular way the boundary conditions are applied and maintained may also influence the system. Those effects, however, are beyond the scope of this paper.

Many experiments have been performed measuring the heat transfer rate through a porous medium bounded by non-ideal plates. These experiments were mostly concerned with determining the heat transport characteristics in the medium once the fluid was convecting and paid little attention to the critical values. Lister [6] mentions in his review paper that some of the data found in the literature were rescaled to show a common location for the onset of convection. Rescaling to match theory may, in fact, invalidate the data. If the theoretical model used is inappropriate for the experimental setup under consideration, rescaling will increase the error in the results. In the present

* Corresponding author.

Nomenclature

a	horizontal wavenumber
c	specific heat
c_a	acceleration coefficient
c_p	specific heat at constant pressure
$d_{u,l}$	upper, lower plate thickness
D	vertical derivative operator, $\partial/\partial z$
$\overline{\mathcal{D}}$	scaled diffusivity tensor of porous medium
Da	Darcy number, K_v/H^2
\vec{g}	gravity
H	height of porous medium
h	heat transfer coefficient
$\hat{i}, \hat{j}, \hat{k}$	unit vectors for x, y, z directions
j	imaginary number, $\sqrt{-1}$
K	scalar permeability
$\overline{\vec{K}}$	permeability tensor of porous medium
$\overline{\mathcal{K}}$	scaled permeability tensor of porous medium
k	scalar conductivity
$\overline{\vec{k}}$	conductivity tensor of porous medium
l, m	component horizontal wavenumbers
P	pressure
Pr	Prandtl number, ν/α_v
q	characteristic values
q''	heat flux
R	Rayleigh number, $g\beta\Delta TH^3/\alpha_v\nu$
Ra	Rayleigh–Darcy number, $g\beta\Delta TK_v H/\alpha_v\nu$
S	arbitrary constant
T	temperature
ΔT	temperature difference across porous medium
t	time
\vec{u}	velocity of fluid
u, v, w	$x, y,$ and z components of velocity
W	vertical velocity perturbation amplitude.

Greek symbols

α	scalar diffusivity
$\overline{\vec{\alpha}}$	diffusivity tensor of porous medium
β	coefficient of thermal expansion
δ_{ij}	Kronecker delta
η	ratio of directional diffusivities, α_h/α_v
ϕ	porosity
$\lambda_{u,l}$	ratio of conductivities, $k_v/k_{u,l}$
μ	dynamic viscosity
ν	kinematic viscosity
ρ	density
ρ_0	reference fluid density
θ	vertically-dependent amplitude of thermal perturbation
ξ	ratio of directional permeabilities, K_h/K_v .

Subscripts

B	bottom edge of bottom plate
b	steady-state value
f	properties of the fluid

h	horizontal direction
l	properties of the lower plate
m	properties of the porous medium
p	perturbation values
T	top edge of top plate
u	properties of the upper plate
v	vertical direction.

paper, we demonstrate that experiments using different horizontal boundaries may have different critical values for the onset of convection.

Analytical expressions for the critical values of convection in an anisotropic porous medium were developed in a series of three papers. In the first, Castinel and Combarous [7] extended the work of Horton–Rogers and Lapwood to media with anisotropic permeability. In a continuation of that work, Epherre [8] added anisotropy in the diffusivity of the porous medium. Each of these assume that the medium is isotropic in both horizontal directions. Finally, Kvernold and Tyvand [9] developed a theory for an anisotropic medium whose principle axes of permeability and diffusivity align with one another but can nonetheless have anisotropy in the horizontal plane.

Close, Symmons, and White [10] were able to obtain experimental results closely matching ideal boundary theory by using a porous medium saturated with a gas. The necessity for other researchers to scale data to match theoretical values for onset, however, calls into question the accuracy of ideal boundary theory for experiments. For this reason, a more accurate model of experimentally realizable situations is necessary to better understand the onset of convection in a porous medium heated from below. This model should reduce the discrepancies between theoretical and experimental critical values. It will also determine the magnitude of the error in assuming ideal plates when dealing with experimental values and give estimates of when the ideal boundary assumptions are valid. The goal of this work is to present a linear stability analysis of Horton–Rogers–Lapwood convection in an infinite horizontal domain that takes into account the effects of the bounding plates as well as the anisotropy in the porous medium. This model is then analyzed and the results are compared to theoretical and experimental works [7,8,11]. Finally, conclusions are drawn as to the applicability of ideal plate theory to experiments based on their bounding plate properties and the effects these plates have on the stability of the no-motion state.

2. Analytical formulation

Fig. 1 shows the problem studied in this paper. A porous medium of infinite horizontal extent is sandwiched between two solid plates. A fluid completely saturates the porous medium. In the figure, the entries on the left side denote the temperatures at (from top to bottom) the top of the upper plate, the interface between the upper plate and the porous medium, the interface between the porous medium and the lower plate, and the bottom of the lower plate. The entries in the middle give the functions of temperature for the five distinct regions; the upper boundary, the upper plate, the porous medium, the lower plate, and the lower boundary. The entries on the right show the height measurements at the top of the upper plate, the upper plate-medium interface, the center of the medium, the lower plate-medium interface, and the bottom of the lower plate. q'' is the flux entering the bottom of

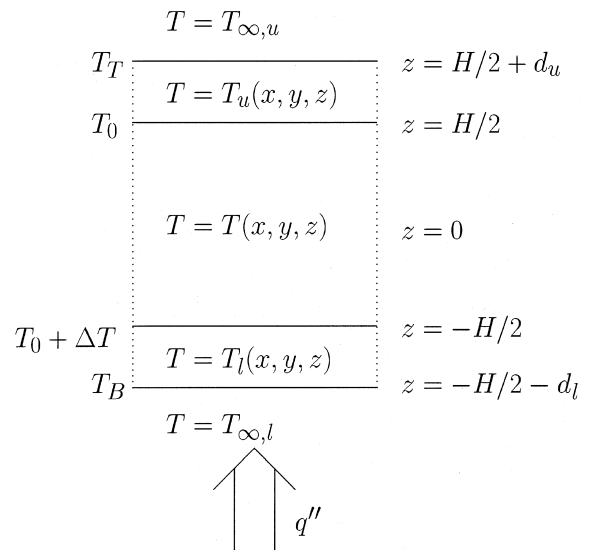


Fig. 1. Schematic of Horton–Rogers–Lapwood convection cell bounded by finite thickness plates of infinite horizontal extent.

the lower plate, $T_{\infty,u}$ is the temperature of the fluid flowing past the upper boundary (cooling bath), and $T_{\infty,l}$ is the temperature of the fluid flowing past the lower boundary (heating bath). Note that T_0 is not a fixed quantity but will change depending on the boundary temperatures ($T_{\infty,u}$ and $T_{\infty,l}$) as well as the heat transfer conditions at the boundaries.

Each of the plates is assumed homogeneous and isotropic with conductivities k_u and k_l and diffusivities α_u and α_l fixed. They are impermeable and immobile. The energy equation for the plates is:

$$\frac{\partial T_{u,l}}{\partial t} = \alpha_{u,l} \nabla^2 T_{u,l} \tag{1}$$

The porous medium, on the other hand, is anisotropic in conductivity (k_h and k_v), diffusivity (α_h and α_v), and permeability (K_h and K_v). Epherre’s model [8]—that the medium is horizontally isotropic—are used here. Kvernfold and Tyvand’s model [9]—that the principle axes of these properties are aligned with each other—is also used. The second-order tensors describing these properties are:

$$\overline{\overline{K}}_m = \begin{bmatrix} k_h & 0 & 0 \\ 0 & k_h & 0 \\ 0 & 0 & k_v \end{bmatrix} \tag{2}$$

$$\overline{\overline{\alpha}}_m = \begin{bmatrix} \alpha_h & 0 & 0 \\ 0 & \alpha_h & 0 \\ 0 & 0 & \alpha_v \end{bmatrix} = \alpha_v \begin{bmatrix} \eta & 0 & 0 \\ 0 & \eta & 0 \\ 0 & 0 & 1 \end{bmatrix} = \alpha_v \overline{\overline{\mathcal{D}}} \tag{3}$$

$$\overline{\overline{K}} = \begin{bmatrix} K_h & 0 & 0 \\ 0 & K_h & 0 \\ 0 & 0 & K_v \end{bmatrix} = K_v \begin{bmatrix} \xi & 0 & 0 \\ 0 & \xi & 0 \\ 0 & 0 & 1 \end{bmatrix} = K_v \overline{\overline{K}} \tag{4}$$

where $\overline{\overline{\mathcal{D}}}$ and $\overline{\overline{\mathcal{K}}}$ are the diffusivity and permeability tensors scaled by their respective vertical components and

$$\eta = \frac{\alpha_h}{\alpha_v} \quad \xi = \frac{K_h}{K_v} \tag{6}$$

With these tensors in mind, the mass, momentum, and energy equations used by Horton and Rogers [3] can be rewritten by combining aspects of previous work done by Castinel and Combarous [7], Nield and Bejan [12], and Kvernfold and Tyvand [9]. Castinel and Combarous assume that the permeability is anisotropic, but keep the conductivity isotropic. Nield and Bejan assume the porous medium is isotropic, but use the more precise acceleration coefficient (c_a) term with the momentum instead of the inverse porosity (ϕ^{-1}). Kvernfold and Tyvand use anisotropic tensors for both permeability and diffusivity but do not include any velocity derivatives in the momentum

term. Combining the anisotropy with the acceleration coefficient yields:

$$\phi \frac{\partial \rho_f}{\partial t} + \nabla(\rho_f \vec{u}) = 0 \quad \text{mass} \tag{7}$$

$$\rho_f c_a \frac{\partial \vec{u}}{\partial t} + \mu \overline{\overline{K}}^{-1} \cdot \vec{u} = \rho_f \vec{g} - \nabla P \quad \text{momentum} \tag{8}$$

$$(\rho c)_m \frac{\partial T}{\partial t} + \nabla \cdot [(\rho c_p)_f T \vec{u}] = \nabla \cdot (\overline{\overline{k}}_m \nabla T) \quad \text{energy} \tag{9}$$

There are three assumptions that will simplify the above equations. First is the Oberbeck–Boussinesq approximation [13,14], which states that the fluid density is constant except where acted upon by a body force. Next the diffusivity, specific heat, and density are assumed constant except where the density modifies the action of a body force. Finally, the time derivative in the momentum equation is neglected because of the scale of c_a . Nield and Bejan [12] argue that even the largest values of c_a yield decay times much smaller than 1 s. The diffusion time, $\tau = H^2/\alpha_v$, for a typical experiment is on the order of 10^3 s, so the effects of transients die away quickly compared to the time scale of the thermal relaxation. Shattuck et al. [15] also neglected the acceleration term after determining the coefficient on that term was several orders of magnitude smaller than other terms for common experimental values.

After premultiplying the terms of the momentum equation by $\overline{\overline{K}}/\mu$ and applying the assumptions listed above, the resulting equations of mass, momentum, and energy for the porous medium are:

$$\nabla \cdot \vec{u} = 0 \tag{10}$$

$$\vec{u} = \rho_0 [1 - \beta(T - T_0)] \frac{\overline{\overline{K}} \cdot \vec{g}}{\mu} - \frac{\overline{\overline{K}} \cdot \nabla P}{\mu} \tag{11}$$

$$(\rho c)_m \frac{\partial T}{\partial t} + (\rho c_p) \vec{u} \cdot \nabla T = \nabla \cdot (\overline{\overline{k}}_m \nabla T) \tag{12}$$

where β is the coefficient of volumetric thermal expansion.

The third equation has an important assumption embedded in it. It is only valid if the porous matrix and the saturating fluid are in local thermal equilibrium. If the conductivities of the solid and the fluid are vastly different, this assumption may be false and the equation may give inaccurate results.

There are six boundary conditions for this problem. The first two are at the extreme edge of the solid plates. The most general condition is given at the upper boundary of the upper plate as:

$$\frac{\partial T}{\partial z} \Big|_{z=H/2+d_u} + \frac{Bi_u}{d_u} T_u(H/2 + d_u) = \frac{Bi_u}{d_u} T_{\infty,u} \quad (13)$$

where the Biot number $Bi_{u,1}$ is defined as:

$$Bi_{u,1} = \frac{hd_{u,1}}{k} \quad (14)$$

The lower edge can be modeled with a Biot condition taking care to note the *direction* of the flux as follows:

$$\frac{\partial T_1}{\partial z} \Big|_{z=-H/2-d_1} - \frac{Bi_1}{d_1} T_1(-H/2 - d_1) = -\frac{Bi_1}{d_1} T_{\infty,1} \quad (15)$$

Setting the Bi number for each plate to different values can change the nature of the boundary conditions. Many experiments report a constant boundary temperature condition, which corresponds to $Bi = \infty$. Other experiments use a constant *flux* condition [16], particularly when electrically heating the lower boundary. This condition cannot be represented by the general conditions above but rather by:

$$\frac{\partial T_u}{\partial z} \Big|_{z=H/2+d_u} = c_u \quad \frac{\partial T_1}{\partial z} \Big|_{z=-H/2-d_1} = c_1$$

where $c_{u,1}$ are constants.

The interfaces between the porous medium and the plates have two thermal boundary equations each. The first is a requirement that the temperature is continuous across the interface:

$$T_u(H/2) = T(H/2) \quad T_1(-H/2) = T(-H/2) \quad (16)$$

The second is that the heat flux is continuous across the interface:

$$k_u \frac{\partial T_u}{\partial z} \Big|_{z=H/2} = k_v \frac{\partial T}{\partial z} \Big|_{z=H/2} \quad (17)$$

$$k_1 \frac{\partial T_1}{\partial z} \Big|_{z=-H/2} = k_v \frac{\partial T}{\partial z} \Big|_{z=-H/2}$$

Finally, there is an impermeability condition at the interface that requires the vertical component of velocity at the interfaces to be zero:

$$w(H/2) = 0 \quad w(-H/2) = 0 \quad (18)$$

Performing linear stability analysis requires knowledge of the conduction state about which we perturb the solution. This solution assumes the fluid is stationary in the porous medium. This gives an *a priori* steady-state fluid velocity of:

$$\vec{u}_b = \vec{0} \quad (19)$$

Using Eq. (12), and the boundary conditions in Fig. 1, the steady-state temperature profile for the porous

medium is:

$$T_b = T_0 + \Delta T \left(\frac{1}{2} - \frac{z}{H} \right) \quad (20)$$

In the boundaries, the one-dimensional conduction equation applies. Assuming perfect thermal contact between the outer edges of the plates and the cooling and heating baths ($Bi_{u,1} = \infty$), this gives a general solution for plate temperature of:

$$T_{u,b} = \frac{(z - H/2)}{d_u} (T_T - T_0) + T_0 \quad (21)$$

$$T_{1,b} = -\frac{(z + H/2)}{d_1} (T_B - T_0 - \Delta T) + T_0 + \Delta T \quad (22)$$

It is important to note that while ΔT , T_0 , and q'' are not explicitly known, their steady state values can be determined as functions of $T_{T,B}$, $Bi_{u,1}$, and the thermal properties of the plates and of the matrix. Specifically, for perfect thermal contact between the plates and the baths:

$$q'' = \frac{T_B - T_T}{\frac{d_1}{k_1} + \frac{H}{k_v} + \frac{d_u}{k_u}} \quad \Delta T = \frac{q'' H}{k_v} \quad (23)$$

$$T_0 = T_T + \frac{q'' d_u}{k_u}$$

The only remaining variable is the pressure. Using Eq. (11) and the steady-state values found above, the pressure is given by:

$$P_b = -g\rho_0 z + \frac{g\rho_0 \beta \Delta T z}{2} - \frac{g\rho_0 \beta \Delta T z^2}{2H} + C_1 \quad (24)$$

where C_1 is an arbitrary constant. Finally, taking the pressure at the center of the porous medium to be P_0 , the no-flow pressure profile is:

$$P_b = P_0 - g\rho_0 \left[z + \frac{\beta \Delta T}{2} \left(\frac{z^2}{2} - z \right) \right] \quad (25)$$

At this point, it is helpful to scale and nondimensionalize the variables in the three main equations and the three steady-state solutions. Below, the primed variables are those which have been scaled and the unprimed are the original variables. The scales are:

$$x'_i = \frac{x_i}{H} \quad t' = t \left(\frac{\alpha_v}{H^2} \right) \quad u'_i = u_i \left(\frac{H}{\alpha_v} \right)$$

$$P' = P \left(\frac{K_v}{\rho_0 v \alpha_v} \right) \quad T' = \frac{T - T_0}{\Delta T}$$

The equations of mass, momentum, and energy in the

new variables are:

$$\nabla' \cdot \vec{u}' = 0 \quad \text{mass} \tag{26}$$

$$\vec{u}' = -\frac{gHK_v}{\alpha_v \nu} (1 - \beta \Delta T T') \vec{\mathcal{K}} \cdot \hat{k} - \vec{\mathcal{K}} \cdot \nabla' P' \tag{27}$$

momentum

$$\sigma \frac{\partial T'}{\partial t'} + \vec{u}' \cdot \nabla' T' = \nabla' \cdot (\vec{\mathcal{D}} \cdot \nabla' T') \quad \text{energy} \tag{28}$$

where $\sigma = (\rho c)_m / (\rho c)_f$ is the heat capacity ratio [12].

A linear stability analysis can now be performed on the scaled and nondimensionalized variables by assuming each variable is made up of a steady-state and a perturbed component. For the sake of clarity, the primes denoting scaled variables will be dropped throughout the rest of the paper. As an example, the temperature can be represented as:

$$T = T_p + T_b \tag{29}$$

where T_p is the perturbation amplitude and T_b is the steady-state value. Substituting these combinations into the mass, momentum, and energy equations and eliminating second-order terms yields:

$$\nabla \cdot \vec{u}_p = 0 \tag{30}$$

$$\vec{u}_p = Ra T_p \vec{\mathcal{K}} \cdot \hat{k} - \vec{\mathcal{K}} \cdot \nabla P_p \tag{31}$$

$$\sigma \frac{\partial T_p}{\partial t} - w_p = \nabla \cdot (\vec{\mathcal{D}} \cdot \nabla T_p) \tag{32}$$

where Ra is the Rayleigh–Darcy number:

$$Ra = R Da = \frac{g\beta\Delta TH^3}{\alpha_v \nu} \frac{K_v}{H^2} = \frac{g\beta\Delta THK_v}{\alpha_v \nu} \tag{33}$$

Expanding the divergence operation in Eq. (30) gives:

$$\frac{\partial u_p}{\partial x} + \frac{\partial v_p}{\partial y} + \frac{\partial w_p}{\partial z} = 0 \tag{34}$$

Taking the double curl of Eq. (31) to eliminate pressure terms, using the conservation of mass equation above to eliminate u_p and v_p terms, and extracting the \hat{k} component yields:

$$\begin{aligned} & \left(\xi \frac{\partial^2}{\partial x^2} + \xi \frac{\partial^2}{\partial y^2} + \frac{\partial^2}{\partial z^2} \right) w_p \\ & = Ra \xi \left(\frac{\partial^2}{\partial x^2} + \frac{\partial^2}{\partial y^2} \right) T_p \end{aligned} \tag{35}$$

Finally, expanding the divergence operators in (32) produces:

$$\sigma \frac{\partial T_p}{\partial t} - w_p = \left(\eta \frac{\partial^2}{\partial x^2} + \eta \frac{\partial^2}{\partial y^2} + \frac{\partial^2}{\partial z^2} \right) T_p \tag{36}$$

Now the momentum and energy equations contain only two unknown scalars, w_p and T_p . The linearity of these equations allows a separation of variables:

$$w_p = W(z)E(x, y, t) \tag{37}$$

$$T_p = \theta(z)E(x, y, t) \tag{38}$$

where $E(x, y, t) = \exp(jlx + jmy + st)$ with l and m being horizontal wave numbers and s being the growth rate.

Substituting these representations into the momentum and energy equation, using D as the vertical derivative operator, combining the horizontal wavenumbers into an overall horizontal wavenumber [12] $a = \sqrt{l^2 + m^2}$, and dividing by $E(x, y, t)$ gives:

$$(-\xi a^2 + D^2)W(z) = -Ra \xi a^2 \theta(z) \tag{39}$$

$$-W(z) = (-\eta a^2 + D^2 - \sigma s)\theta(z) \tag{40}$$

Eliminating $W(z)$ between the equations leaves:

$$(D^2 - \xi a^2)(D^2 - \eta a^2 - \sigma s)\theta(z) = Ra \xi a^2 \theta(z) \tag{41}$$

Marginal stability occurs when the real part of the growth rate s is zero. Given that, the characteristic values for marginal stability which solve Eq. (41) are:

$$q_1 = \sqrt{a^2 \left(\frac{\xi + \eta}{2} \right) + \sqrt{a^4 \left(\frac{\xi - \eta}{2} \right)^2 + a^2 Ra \xi}} \tag{42}$$

$$q_2 = \sqrt{a^2 \left(\frac{\xi + \eta}{2} \right) + \sqrt{a^4 \left(\frac{\xi - \eta}{2} \right)^2 + a^2 Ra \xi}} \tag{43}$$

where

$$\frac{dW(z)}{dz} = qW(z)$$

and the z -dependent terms of the separated temperature and velocity solutions can be written as:

$$\begin{aligned} \theta(z) = & C_1 \cosh(q_1 z) + S_1 \sinh(q_1 z) + \\ & C_2 \cosh(q_2 z) + S_2 \sinh(q_2 z) \end{aligned} \tag{44}$$

$$W(z) = C_{1w} \cosh(q_1 z) + S_{1w} \sinh(q_1 z) + C_{2w} \cosh(q_2 z) + S_{2w} \sinh(q_2 z) \tag{45}$$

For the plates, perturbations in the plate-porous medium temperature profile mean three-dimensional conduction in the plate is possible. The conduction equation in the plates is therefore:

$$\nabla^2 T_{u,i} = \frac{1}{\alpha_{u,i}} \frac{\partial T_{u,i}}{\partial t} \tag{46}$$

By separating the temperature into two variables—one with horizontal dependence and one with vertical—a general solution can be formed:

$$\theta_u(z) = E(x, y, t)[C_3 \cosh(az) + S_3 \sinh(az)] \tag{47}$$

$$\theta_l(z) = E(x, y, t)[C_4 \cosh(az) + S_4 \sinh(az)] \tag{48}$$

where a is the overall horizontal wavenumber from before. The $E(x, y, t)$ function models the horizontal dependence of $\theta_{u,i}$ in order to satisfy temperature continuity on the porous medium-plate interfaces.

Finally, the boundary and matching conditions can be written in terms of three variables; the temperature perturbation of the porous medium θ and the temperature perturbations of the plates $\theta_{u,i}$. The eight boundary equations require:

temperature continuity across the porous medium-plate interfaces;

$$\theta(1/2) = \theta_u(1/2) \quad \theta(-1/2) = \theta_l(-1/2) \tag{49}$$

flux continuity through the porous medium-plate interfaces;

$$\left. \frac{d\theta}{dz} \right|_{z=1/2} = \frac{1}{\lambda_u} \left. \frac{d\theta_u}{dz} \right|_{z=1/2} \quad \left. \frac{d\theta}{dz} \right|_{z=-1/2} = \frac{1}{\lambda_l} \left. \frac{d\theta_l}{dz} \right|_{z=-1/2} \tag{50}$$

no vertical component of velocity at the porous medium-plate interfaces;

$$W(1/2) = (D^2 - \eta a^2)\theta(1/2) = 0$$

$$W(-1/2) = (D^2 - \eta a^2)\theta(-1/2) = 0 \tag{51}$$

and compliance with the Biot boundary conditions;

$$\left. \frac{d\theta_u}{dz} \right|_{z=1/2+d_u} + \frac{H}{d_u} Bi_u \theta_u(1/2 + d_u) = 0 \tag{52}$$

$$\left. \frac{d\theta_l}{dz} \right|_{z=-1/2+d_l} - \frac{H}{d_l} Bi_l \theta_l(-1/2 - d_l) = 0$$

Note that the specific Biot conditions chosen for this

study are $Bi_{u,i} = \infty$. This allows for comparison with a number of experiments in the literature.

The linearized equations of motion can be written into a matrix equation

$$\mathbf{A} \vec{C} = \vec{0} \tag{53}$$

where \mathbf{A} is a matrix containing the hyperbolic terms of the temperature solutions θ , θ_u , and θ_l , and \vec{C} is a column vector containing the coefficients C_i and S_i :

$$\vec{C} = [C_1, S_1, C_2, S_2, C_3, S_3, C_4, S_4]^T \tag{54}$$

There are two general cases for which Eq. (53) is true; either the entries in \vec{C} are all 0—meaning no perturbation amplitude and thus no convection—or the determinant of \mathbf{A} is 0. The first case is the conduction solution. The second case is the more interesting situation as it denotes the critical point where the conduction solution becomes unstable.

The critical values of the Rayleigh–Darcy number and wave number can be found by obtaining the values for which the determinant of \mathbf{A} is 0 in ten-dimensional parameter space and minimizing the Rayleigh–Darcy number. In other words, the solution will be found on the surface:

$$F(Ra, a, d_l, d_u, \lambda_l, \lambda_u, \eta, \zeta, Bi_l, Bi_u) = 0 \tag{55}$$

where

$$F = \det(\mathbf{A}) \tag{56}$$

and the *critical* value will be determined by the minimum Ra of those curves.

3. Results and discussion

The critical Ra and a values are found using a continuation method [17]. The program is given initial values for Bi_u , Bi_l , d_u , d_l , λ_u , and λ_l . Initial guesses for Ra_c and a_c are calculated using Epherre’s equations for ideal boundaries and horizontally isotropic plates [8]

$$Ra_c = \pi^2 \left[\left(\frac{\eta}{\zeta} \right)^{1/2} + 1 \right]^2 \tag{57}$$

$$a_c = \pi(\zeta\eta)^{-1/4} \tag{58}$$

Once a critical point for this configuration is found, one of the ten parameters is changed and a new critical value set found. This decreases computation time in that the program is well adapted to working with small changes in a single parameter.

The first results of the program are used to test its

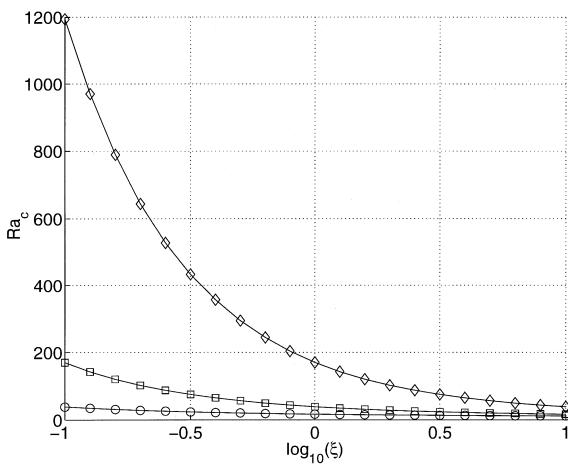


Fig. 2. Comparison of Epherre's theoretical value (solid line) of Ra_c and computed value using 'ideal' plates. The computed values are for $\eta = 10^{-1}$ (○), $\eta = 10^0$ (□), and $\eta = 10^1$ (◇).

accuracy vs other theory. Parameters closely matching those for ideal plates are used and the results compared with Epherre's equations. The parameters are:

$$Bi_u = Bi_l = \infty \quad d_u = d_l = 10^{-3} \quad \lambda_u = \lambda_l = 10^{-4}$$

Runs are made using ξ and η values between 0.1 and 10.0. Fig. 2 shows the comparison between the calculated and theoretical values for Ra_c . Fig. 3 shows the same comparison for the critical wave number. In both cases, the calculated value matches almost exactly to the ideal plate theory from Epherre.

The first new results we present are for a porous

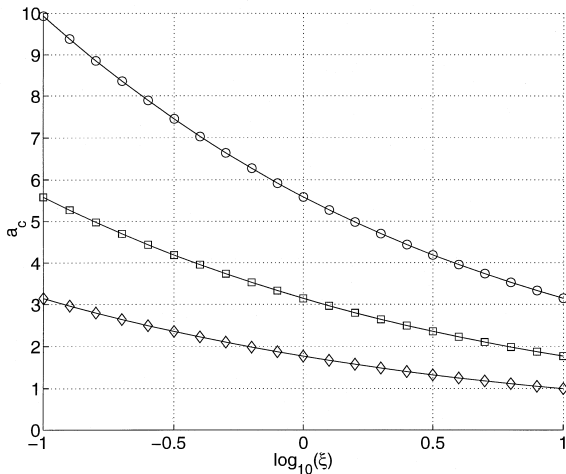


Fig. 3. Comparison of Epherre's theoretical value (solid line) of a_c and computed value using 'ideal' plates. The computed values are for $\eta = 10^{-1}$ (○), $\eta = 10^0$ (□), and $\eta = 10^1$ (◇).

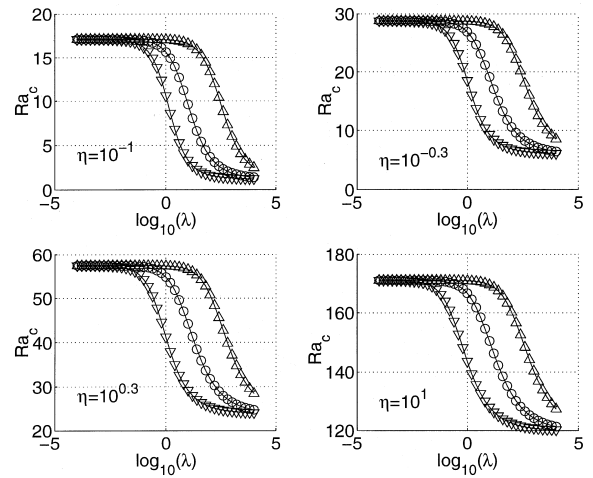


Fig. 4. Ra_c for a porous medium with isotropic permeability ($\xi = 1$) bounded by plates of various thicknesses and diffusivities. Within each group, the left curve (∇) has $d = 1.0$, the middle (\square) has $d = 10^{-1.5}$, and the right (\triangle) has $d = 10^{-3}$. The diffusivity ratio is displayed in the figure. The solid line is shown to connect the computed values and does not denote theoretical data. Note that the horizontal axes of the four plots are the same, but the vertical axes are different.

medium with isotropic permeability ($\xi = 1$) but varying diffusivity ratios (η). For simplicity, the boundary plates are assumed to be identical to one another. Fig. 4 shows several families of Ra_c curves. Curves with similar symbols have the same d values. Within each plot, the right-most curve is for $d = 10^{-3}$, the middle for $d = 10^{-1.5}$, and the left-most for $d = 1.0$ where d is the scaled thickness of the plates. The thermal boundary condition on each plate is $Bi = \infty$, meaning the temperature is held constant at the outer edge and there is perfect thermal contact between the baths and the plates.

This figure looks qualitatively like the figures presented by Metcalfe and Beringer [18] for Rayleigh-Bénard convection in bounded cryogenic experiments. Convection in a porous medium has the same decrease in stability as either the plate thickness increases or the medium conductivity increases. Although the actual numbers are different, the *shape* of the curve is similar. It is clear that the degree of diffusive anisotropy contributes to a shift in critical Ra values. This follows Epherre's conclusion that Ra_c is dependent on η . A porous medium with a higher horizontal diffusivity, then, would tend to be able to withstand a greater temperature gradient before convection occurs.

This figure also shows the influence of the plate thickness in determining the stability of the no-motion state. If the medium is bounded by thick plates, the onset of convection is likely to occur earlier than in a medium bounded by thinner plates. The variation in

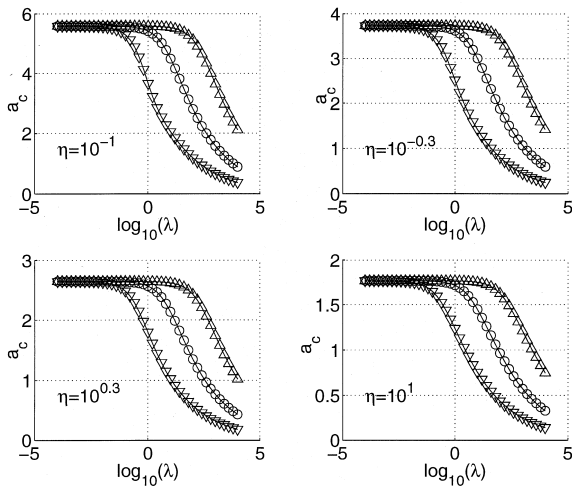


Fig. 5. a_c for a porous medium with isotropic permeability ($\xi=1$) bounded by plates of various thicknesses and diffusivities. Within each group, the left curve (∇) has $d=1.0$, the middle (\square) has $d=10^{-1.5}$, and the right (\triangle) has $d=10^{-3}$. The diffusivity ratio is displayed in the figure. The solid line is shown to connect the computed values and does not denote theoretical data. Note that the horizontal axes of the four plots are the same, but the vertical axes are different.

critical Ra with d occurs over a fairly wide band in λ , and must therefore be taken into account when attempting to compare experiment with theory. Fig. 5

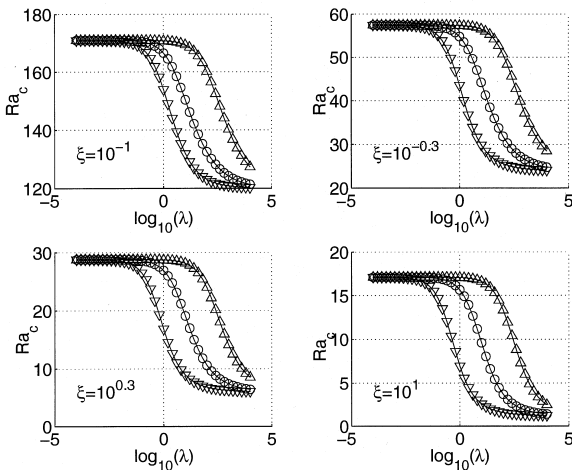


Fig. 6. Ra_c for a porous medium with isotropic diffusivity ($\eta=1$) bounded by plates of various thicknesses and conductivities. Within each group, the left curve (∇) has $d=1.0$, the middle (\square) has $d=10^{-1.5}$, and the right (\triangle) has $d=10^{-3}$. The permeability ratio is displayed in the figure. The solid line is shown to connect the computed values and does not denote theoretical data. Note that the horizontal axes of the four plots are the same, but the vertical axes are different.

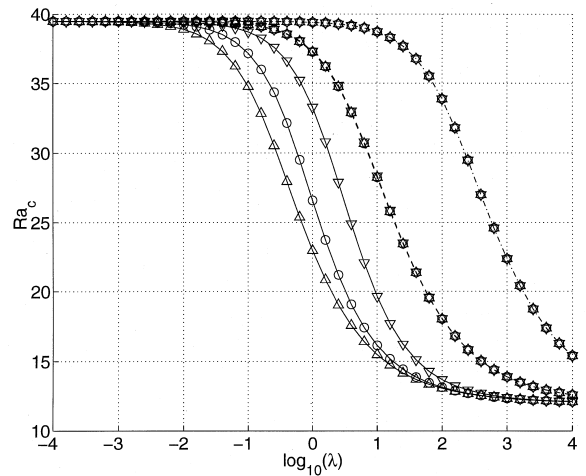


Fig. 7. Ra_c for a porous medium with $\eta/\xi=1$. The line styles denote: $d=1.0$ ($-$), $d=10^{-1.5}$ ($-$), $d=10^{-3}$ ($-$). The symbols are: $\xi=\eta=10^{-1}$ (∇), $\xi=\eta=1$ (\circ), and $\xi=\eta=10^1$ (\triangle). The solid line is shown to connect the computed values and does not denote theoretical data.

shows values for the critical wave numbers given the same parameters as above. Again, each family of curve has the same shape, but the average value is shifted up or down depending on the value of η . For the wave number, however, a higher relative horizontal diffusivity in the medium causes a decrease in the critical wavenumber. This means that whenever the critical Ra is reached, the length scale of the ensuing convection would be larger in media with higher horizontal diffusivities.

The next parameter we explore is the permeability ratio. Fig. 6 shows several families of Ra_c curves for different values of the permeability ratio (ξ) while the diffusivity is kept isotropic ($\eta=1$). Again, the right-most curve is for $d=10^{-3}$, the middle for $d=10^{-1.5}$, and the left-most for $d=1.0$ with temperature held fixed at the extreme boundaries. These curves appear to be the same shape as those in Fig. 4. The notable exception is the location of the curves relative to each other. In this case, an increase in the horizontal component of K_m causes a decrease in Ra_c . This follows Epherre's equations, since critical Ra is dependent on ξ with a negative power.

Fig. 7 shows several families of curves for which η/ξ are equal. An upward-pointing triangle denotes a curve where the horizontal components of ξ and η are ten times that of the vertical, a square indicates isotropic values of diffusivity and permeability, and a downward-pointing triangle denotes ξ and η equal to 0.1. There seem to be only five curves, but in actuality there are nine. The three that lose stability first are for very thick ($d=1.0$) plates. The next three are for

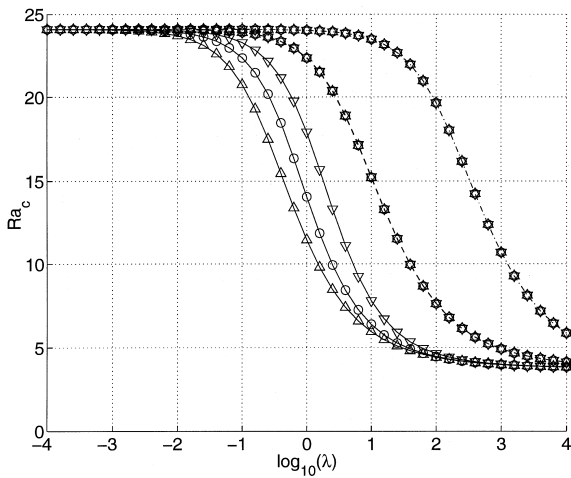


Fig. 8. Ra_c for a porous medium with $\eta/\zeta = 10^{-0.5}$. The line styles denote: $d = 1.0$ (—), $d = 10^{-1.5}$ (—), $d = 10^{-3}$ (—). The symbols are: $\eta = 10^{-1}$, $\zeta = 10^{-0.5}$ (∇); $\eta = 10^{-0.5}$, $\zeta = 10^{-0.3}$, $\zeta = 10^{0.2}$ (\circ); and $\eta = 10^{0.5}$, $\zeta = 10^1$ (\triangle). The solid line is shown to connect the computed values and does not denote theoretical data.

$d = 10^{-1.5}$ thick plates, and show that for this thickness the individual values of ζ and η are unimportant—only their ratio matters. The most stable curves also fall on top of each other, and are for a plate thickness $d = 10^{-3}$. Fig. 8 shows another set of nine curves, this time with a constant η/ζ ratio of $10^{-0.5}$. Again, the

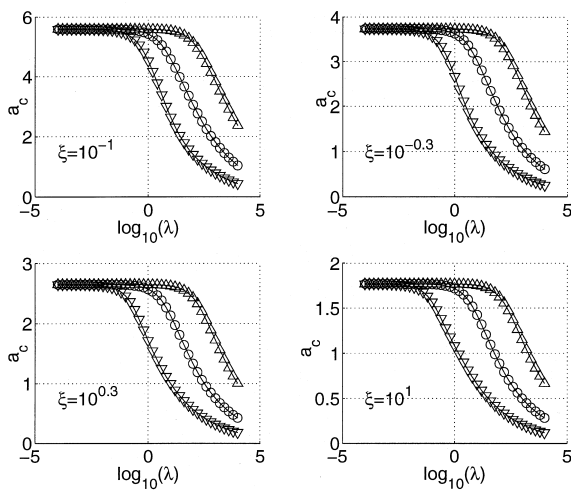


Fig. 9. a_c for a porous medium with isotropic diffusivity ($\eta = 1$) bounded by plates of various thickness and conductivity. Within each group, the left curve (∇) has $d = 1.0$, the middle (\square) has $d = 10^{-1.5}$, and the right (\triangle) has $d = 10^{-3}$. The permeability ratio is displayed in the figure. The solid line is shown to connect the computed values and does not denote theoretical data. Note that the horizontal axes of the four plots are the same, but the vertical axes are different.

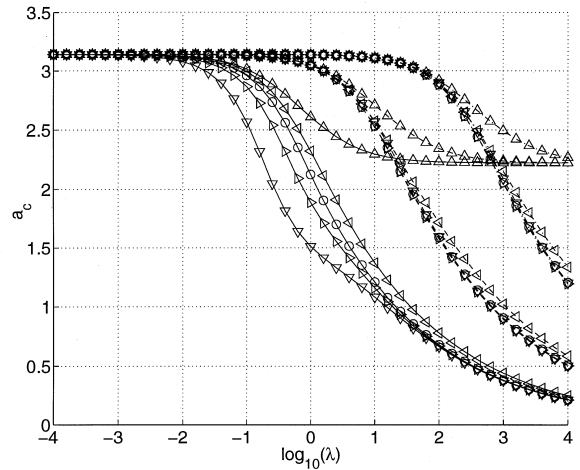


Fig. 10. a_c for a porous medium with $\eta\zeta = 1$. The line styles denote: $d = 1.0$ (—), $d = 10^{-1.5}$ (—), $d = 10^{-3}$ (—). The symbols are: $\eta = 10^{-1}$, $\zeta = 10^1$ (∇); $\eta = 10^{-0.5}$, $\zeta = 10^{0.5}$ (\triangleright); $\eta = 1$, $\zeta = 1$ (\circ); $\eta = 10^{0.5}$, $\zeta = 10^{-0.5}$ (\triangleleft); and $\eta = 10^1$, $\zeta = 10^{-1}$ (\triangle). The solid line is shown to connect the computed values and does not denote theoretical data.

actual values of η and ζ only affect the critical Ra when the plates are very thick.

Fig. 9 shows several families of a_c for different ζ . These curves again have the same shape as their counterparts in Fig. 5. This follows from the theory that a_c is inversely proportional to both ζ and η . Fig. 10 shows the a_c curves for several configurations where $\eta\zeta$ are equal. Again, only the thickest of plates shows a significant difference between the a_c values for equivalent $\eta\zeta$ groups. The notable exceptions are the curves where $\eta = 10$ and $\zeta = 0.1$. These have a much higher-valued asymptote than the others. Running the computer program through $\lambda = 10^{12}$ failed to show any decrease in a_c beyond the value shown at $\lambda = 10^4$.

Although there is very little precision data in the literature that accurately report critical values, comparison with what is available is promising. Howle [11] reports an experiment performed using a porous medium whose properties are:

$$d_l = 4.2 \quad \lambda_l = 0.0025 \quad \zeta = 0.38$$

$$d_u = 0.7 \quad \lambda_u = 0.25 \quad \eta = 1.52$$

Epherre's theory predicts a critical Rayleigh–Darcy number of 22.5. Howle's measured values fell in the range of $Ra_c = 18 \pm 4$. Our stability model gives a value of $Ra_c = 18.62$. Results were also obtained in the same experiment with a different medium

$$d_l = 4.2 \quad \lambda_l = 0.0025 \quad \zeta = 1.25$$

$$d_u = 0.7 \quad \lambda_u = 0.25 \quad \eta = 1.277$$

Epherre's theory predicts $Ra_c = 39.1$. Our new theory's prediction of $Ra_c = 34.2$ is much closer to Howle's measured value of $Ra_c = 32 \pm 4$. These results show the important role that the bounding plates play in modifying the critical Rayleigh–Darcy number.

4. Conclusions

A systematic study of the critical values of an anisotropic porous medium sandwiched between finite property solid plates reveals the following:

1. The relative conductivity between the porous and the boundary plates has a significant impact on the critical Rayleigh–Darcy number for convection. Far from remaining at a stationary $Ra = 4\pi^2$, severe differences in properties between the medium and the bounding surfaces can reduce the stability of the conduction regime, in some cases by a factor of 10 or more. Because the assumption that the solid matrix and the saturating fluid are in thermal equilibrium breaks down when the fluid and the solid have vastly different conductivities, the equations used for this work will not accurately portray such a porous medium. Given that, it is difficult to construct a medium which has a conductivity exceeding that of the metallic materials typically used for bounding surfaces. For experiments using glass or other transparent materials as boundaries—for visualization purposes—the medium and the boundary plates may have similar conductivities and the system may therefore exhibit a lower critical temperature difference.
2. The relative conductivity between the porous medium and the boundary plates can change the wavenumber of the convection pattern. The greater the relative conductivity of the medium, the larger the wavelength of the critical disturbance and thus the larger the horizontal length scale of the convection at onset.
3. The plate thickness is important in determining the conductivity ratio (λ) at which substantial loss of stability begins. Thicker plates tend to reduce the conductivity ratio at which the value of the critical Rayleigh–Darcy number begins to turn away from ideal plate theory. This means that thicker plates must be more conductive than thin plates to have the same critical values. While the effects are asymptotic, they nonetheless show that experimentalists need to consider both the material properties and the physical dimension of the bounding plates when comparing their critical values to theory.
4. The plate thickness is important in determining

where equal values of $\zeta\eta$ (for a_c) or ξ/η (for Ra_c) have different stabilities. This follows from the data summarized in Figs. 7, 8, and 10. We show that for the thickest plates, the level of anisotropy in permeability and diffusivity in the porous medium begin to work independently. In ideal plate theory, a constant product $\zeta\eta$ yields a constant critical wave number and a constant ratio η/ξ yields a constant critical Ra . For thick plates, the individual values of η and ξ influence the stability curve.

The analytical and numerical calculations performed in this work have shown that the physical reality of the boundary plates may play, in some instances, an important role in determining the stability of Horton–Rogers–Lapwood convection. Given that, more work—especially experimental—must be done both to verify these results and to investigate the effects of the boundary plates on heat transport. For experiments dealing with fluids bounded by metal plates, however, the loss in stability caused by the plates themselves is negligible. Only situations where relatively highly conductive porous matrices are bounded by relatively insulating plates or thick plates need to be carefully examined.

We will continue the progress of this paper by conducting experiments to compare the results with new theory. We are working on this through the use of shadowgraphic technology and a specialized porous medium constructed to allow visualization [19]. The relative thicknesses of the boundary materials can easily be changed, as can the relative conductivities by either changing the material in the bounding plates or the fluid used in the porous medium.

Acknowledgements

The authors would like to thank the Donors of The Petroleum Research Fund, administered by the American Chemical Society, for partial support of the work through Grant No. ACS-PRF 31645-G9. MRG would like to acknowledge the support of the National Science Foundation through Grant No. EEC-9256573. We would also like to thank one of the reviewers for several helpful comments.

References

- [1] I. Catton, Natural convection in enclosures, in: Proceedings of the Sixth International Heat Transfer Conference, vol. 6, 1978, pp. 13–31.
- [2] B. Gebhart, Buoyancy-Induced Flows and Transport, Hemisphere, New York, 1988.
- [3] C.W. Horton, F.T. Rogers, Convection currents in a

- porous medium, *Journal of Applied Physics* 16 (1945) 367–370.
- [4] E.R. Lapwood, Convection of a fluid in a porous medium, in: *Proceedings of the Cambridge Philosophical Society*, 1948.
- [5] N. Riahi, Nonlinear convection in a porous layer with finite conducting boundaries, *Journal of Fluid Mechanics* 129 (1983) 153–171.
- [6] C.R.B. Lister, An explanation for the multivalued heat transport found experimentally for convection in a porous medium, *Journal of Fluid Mechanics* 214 (1990) 287–320.
- [7] G. Castinel, M. Combarous, Natural convection in an anisotropic porous layer, *Revue Générale de Thermique* 168 (1975) 937–947 (English translation, *International Chemical Engineering*, 17: 605–614, 1977).
- [8] J.F. Epherre, Criterion for the appearance of natural convection in an anisotropic porous layer, *Revue Générale de Thermique* (1975) 949–950 (English translation, *International Chemical Engineering*, 17: 615–616, 1977).
- [9] O. Kvernfold, P.A. Tyvand, Nonlinear thermal convection in anisotropic porous media, *Journal of Fluid Mechanics* 90 (1979) 609–624.
- [10] D.J. Close, J.G. Symmons, R.F. White, Convective heat transfer in shallow, gas-filled porous media: experimental investigation, *International Journal of Heat and Mass Transfer* 28 (1985) 2371–2378.
- [11] L.E. Howle, Pattern formation at the onset of convection in porous media, Ph.D. thesis, Duke University 1993.
- [12] D.A. Nield, A. Bejan, *Convection in Porous Media*, Springer-Verlag, New York, 1992.
- [13] A. Oberbeck, Über die Wärmeleitung der Flüssigkeiten bei Berücksichtigung der Strömungen infolge von Temperaturdifferenzen, *Annalen der Physik und Chemie* 37 (1879) 271–292.
- [14] J. Boussinesq, in: *Théorie Analytique de la Chaleur*, vol. 2, Gauthier-Villars, Paris, 1903.
- [15] M.D. Shattuck, R.P. Behringer, G.A. Johnson, J.G. Georgiadis, Convection and flow in porous media, I: Visualization by magnetic resonance imaging, *Journal of Fluid Mechanics* 332 (1997) 215–245.
- [16] L.E. Howle, R.P. Behringer, J. Georgiadis, Visualization of convective fluid flow in a porous medium, *Nature* 362 (1993) 230–232.
- [17] M. Kubiček, M. Marek, *Computational Methods in Bifurcation Theory and Dissipative Structures*, Springer-Verlag, New York, 1983.
- [18] G.P. Metcalfe, R.P. Behringer, Critical Rayleigh numbers for cryogenic experiments, *Journal of Low Temperature Physics* 78 (1990) 231–246.
- [19] L.E. Howle, R.P. Behringer, J.G. Georgiadis, Convective pattern visualization in order and disorder porous layers, *Journal of Fluid Mechanics* 232 (1997) 247–262.